

THERMOPHYSICAL PROPERTIES  
OF MATERIALS

# Numerical Simulation of Heating an Aluminum Film on Two-Layer Graphene

A. E. Galashev and O. R. Rakhmanova

*Institute of Industrial Ecology, Ural Branch, Russian Academy of Sciences, Yekaterinburg, Russia*

*e-mail: galashev@esko.uran.ru*

Received June 6, 2013

**Abstract**—The behavior of a monolayer aluminum film on two-layer graphene upon heating from 300 to 3300 K was studied by the molecular dynamics method. A stretched film is nonuniformly contracted with an increase in temperature. Aluminum atoms remain on graphene even at 3300 K. Heating reduces stresses in the film plane. Upon heating to 3000 K, the long-range order in graphene is transformed into the mid-range one. The increase in the intensity of vertical displacements of C atoms in one graphene sheet (caused by an increase in temperature) generally reduces the corresponding intensity in the other sheet, whereas the horizontal components of mobility, with few exceptions, behave similarly. Upon heating, stresses in the upper graphene sheet decrease with different rates for different directions.

DOI: 10.1134/S0018151X14030110

## INTRODUCTION

Graphene is a two-dimensional sheet of carbon atoms with a honeycomb structure. Graphene enters the composition of other allotropic carbon modifications (such as graphite, carbon nanotubes, and fullerenes). If a honeycomb carbon sheet is cut in a random direction, it has strictly zigzag or armchair-shaped edges (these edges can also alternate). The concept of a graphene edge is of great importance in theoretical and experimental studies for several reasons. For example, carbon nanotubes are formed from bent graphene sheets, whose edges indicate the character of growth or contact formation. In addition, the conductivity and the mechanical, elastic, and chemical properties of graphene nanoribbons depend strongly on the edge properties (the edge profile indicates the internal symmetry of the ribbon). In particular, nanoribbons with zigzag edges exhibit metallic properties, whereas nanoribbons with armchair-shaped edges can be of the metallic or semiconductor type, depending on their width. Moreover, zigzag edges allow for the existence of localized states near the edge, the electrons in which may demonstrate ferromagnetic ordering. For solar-cell applications, graphene microsheets are grown on polymers (to improve the exciton dissociation and increase conductivity [1–3]) and then transported onto silicon.

The general tendency in the production of crystalline silicon solar cells implies the use of wafers that are as thin as possible. The efficiency of solar batteries depends strongly on the rear cell surface. The rear surface in silicon solar cells is most often improved by inducing a rear-surface field. This field is mainly formed due to sintering (in the temperature range

from 1073 to 1273 K) thin (about 10- $\mu\text{m}$  and even 2- $\mu\text{m}$ -thick) aluminum films with silicon [4].

Two-layer graphene has unique electronic properties, which differ from those of single-layer graphene and bulk graphite due to the parabolic dispersion of its particles [5–7]. It was shown experimentally [8] that two-layer graphene is rippled in the same way as single-layer graphene; however, its structure has not been investigated systematically. This ripple may lead to charge inhomogeneity (electron and hole puddles) [9]. The mechanical properties of two-layer graphene are also important because it is representative of crystalline membranes formed by two atomic layers.

The purpose of this study was to analyze the adsorption properties of two-layer graphene with respect to aluminum atoms in a wide temperature range and to determine the structural, kinetic, and mechanical properties of both the deposited metal and the graphene.

## COMPUTER MODEL

Graphene was simulated based on use of the Tersoff potential [10]

$$\phi = \frac{1}{2} \sum_i \sum_{j \neq i} f_c(r_{ij}) \{f_R(r_{ij}) + b_{ij} f_A(r_{ij})\}, \quad (1)$$
$$f_R(r) = A \exp(-\lambda_1 r),$$
$$f_c(r) = \begin{cases} 1, & r < R, \\ \frac{1}{2} + \frac{1}{2} \cos \frac{\pi(r-R)}{S-R}, & R < r < S, \\ 0, & r > S, \end{cases}$$
$$f_A(r) = -B \exp(-\lambda_2 r),$$

$$b_{ij} = \left(1 + \beta^n \zeta_{ij}^n\right), \quad \zeta_{ij} = \sum_{k \neq i, j} f_c(r_{ik})g(\theta_{ijk}),$$

$$g(\theta) = 1 + \frac{c^2}{d^2} - \frac{c^2}{d^2 + (h - \cos\theta)^2}.$$

Here, subscripts  $i, j$ , and  $k$  indicate atoms of the system,  $r_{ij}$  is the length of the  $i$ - $j$  bond, and  $\theta_{ijk}$  is the angle formed by the  $i$ - $j$  and  $j$ - $k$  bonds. The parameters of Eq. (1) (except for  $S$ ) were taken from [10]. The bond length  $S$  was changed from 0.21 to 0.23 nm, while the other parameters of the potential, which corresponds to the C-C interaction, were kept the same. We also applied a weak Lennard-Jones attraction with the parameters from [9] to take into account the C-C interactions at a distance of  $r_{ij} > 0.23$  nm. These variations prevented graphene from cracking at low temperatures. To avoid graphene sheet rotations, a deceleration force  $-\frac{dV_{ij}(\Omega_{kijl})}{dr_{ij}}$  was applied at each graphene

atomic site; here, the torsional potential  $V_{ij}(\Omega_{kijl})$  can be written as [11]

$$V_{ij}^{\text{tors}}(\Omega_{kijl}) = \varepsilon_{kijl} \left[ \frac{256}{405} \cos^{10} \left( \frac{\Omega_{kijl}}{2} \right) - \frac{1}{10} \right],$$

and the torsion angle  $\Omega_{kijl}$  is defined as the angle between planes, one of which is set by the vectors  $\mathbf{r}_{ik}$  and  $\mathbf{r}_{ij}$ , while the other is set by the vectors  $\mathbf{r}_{ij}$  and  $\mathbf{r}_{jl}$ :

$$\cos \Omega_{kijl} = \frac{|\mathbf{r}_{ji} \times \mathbf{r}_{ik}| \cdot |\mathbf{r}_{ij} \times \mathbf{r}_{jl}|}{|\mathbf{r}_{ji} \times \mathbf{r}_{ik}| \cdot |\mathbf{r}_{ij} \times \mathbf{r}_{jl}|}.$$

The barrier height  $\varepsilon_{kijl}$  for torsion was taken from [11]. The Al-Al interaction was represented as the Sutton-Chen potential [12]

$$U^{\text{SC}} = \varepsilon \left[ \frac{1}{2} \sum_i \sum_{j \neq i} V(r_{ij}) - c \sum_i \sqrt{\rho_i} \right],$$

where

$$V(r_{ij}) = (a/r_{ij})^n,$$

$$\rho_i = \sum_{j \neq i} (a/r_{ij})^m.$$

The parameters of the potential  $U^{\text{SC}}$  ( $\varepsilon, a, c, m$ , and  $n$ ) were reported in [12]. The Al-C interactions were given by the Morse potential with the parameters determined in [13].

The stress at the  $i$ th atomic site of metal film is determined as [12]

$$\sigma_{\alpha\beta}(i) = \frac{\varepsilon}{2a^2\Omega_i} \sum_{i \neq j}^k \left[ -n(a/r_{ij})^{n+2} + mc \left( 1/\sqrt{\rho_i} + 1/\sqrt{\rho_j} \right) (a/r_{ij})^{m+2} \right] r_{ij}^{\alpha} r_{ij}^{\beta},$$

where  $\Omega_i$  is the volume per individual atom, which can be associated with the volume of the Voronoi polyhedron for the  $i$ th atom.

To calculate the stress arising in a graphene sheet, the latter was divided into elemental areas. The atomic stresses  $\sigma_J^i(l)$  of the  $l$ th elemental area for each direction ( $x, y$ , and  $z$ ) with the current subscript  $J$  are determined by calculating the kinetic energies of atoms in this area and the projections of the forces  $f_J^i$  exerted on the  $l$ th area from all other atoms

$$\sigma_J^i(l) = \frac{1}{k} \left\langle \sum_i^k \frac{1}{\Omega_i} (m v_J^i v_J^i) \right\rangle + \frac{1}{S_l} \left\langle \sum_i^k (f_J^i) \right\rangle,$$

where  $k$  is the number of atoms per area  $l$ ,  $m$  is the atomic mass,  $v_J^i$  is the  $J$ th velocity projection of the  $i$ th atom, and  $S_l$  is the  $l$ th area. The angle brackets indicate time averaging. The compressive stresses determined in this way may be positive or negative, depending on the direction of forces  $f_J^i$ . This is the difference between microscopic ( $\sigma_J^i(l)$ ) and macroscopic ( $\bar{\sigma}_J < 0$ ) stresses.

Aluminum atoms were initially located on the graphene sheet in the form of a loose (111) plane of the fcc lattice (oriented parallel to the graphene plane) with a distance  $r_{\text{Al-Al}} = 0.633$  nm between neighboring atoms. Al atoms were located strictly against the centers of hexagonal cells formed by carbon atoms; the shortest distance between C and Al atoms,  $r_{\text{C-Al}} = 0.248$  nm, corresponded to the value calculated within the density-functional theory [14]. In a bulk aluminum crystal,  $r_{\text{Al-Al}} = 0.2857$  nm. Therefore, Al films were initially stretched due to the lattice mismatch between graphene and aluminum. The shortest distance between C atoms in graphene is  $r_{\text{C-C}} = 0.142$  nm. Graphene sheets were arranged according to the Bernal stacking (*ABAB*...) in the same way as in bulk graphite. The distance between graphene sheets was chosen to be 0.3347 nm (the value predicted within the density-functional approximation [15]). The interaction between C atoms lying in layers *A* and *B* was considered using the Lennard-Jones potential with the parameters taken from [16]. The motion equations were integrated by the 4th-order Runge-Kutta method with a time step  $\Delta t = 0.1$  fs. The calculation time was  $10^6 \Delta t$  (or 100 ps) for each temperature value. The initial temperature in the calculations was 300 K. After each cycle of  $10^6$  time steps, the temperature of the system was increased by 500 K to carry out the next calculation with the same duration. The final calculation corresponded to 3300 K. The temperature in the model was maintained using a Berendsen thermostat [17]. The total energy of a free single graphene sheet at  $T = 300$  K was found to be  $-7.02$  eV, which is in agree-

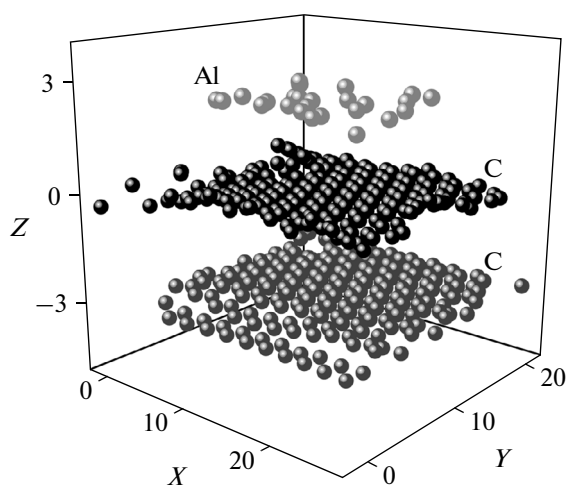


**Fig. 1.** Configuration of the “aluminum film on the two-layer graphene” system corresponding to a temperature of 3300 K at the instant of 100 ps (the coordinates are in angstroms).

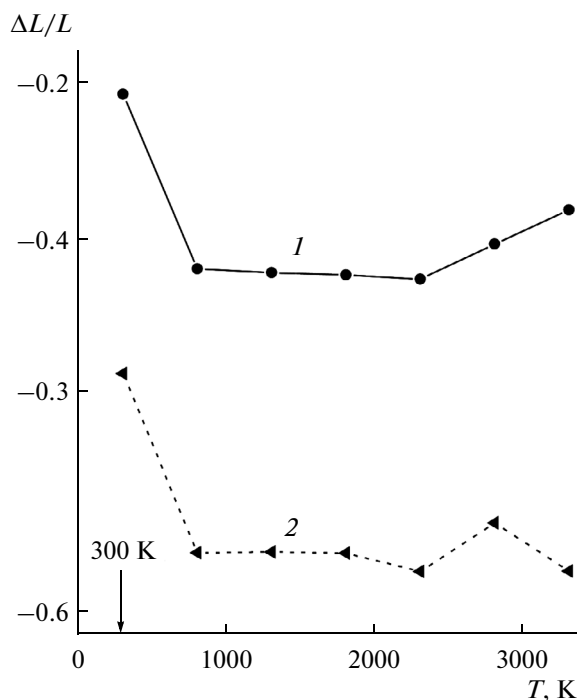


**Fig. 2.** Relative change in the length of Al films in the (1) longitudinal ( $x$ ) and (2) transverse ( $y$ ) directions.

ment with the result of quantum-mechanical calculations ( $-6.98$  eV) [18].

## CALCULATION RESULTS

An analysis of the configuration of the system (Fig. 1) shows that even at  $T = 300$  K Al atoms are combined into a dense flat fragment, although there are still some atoms beyond this fragment. The  $ox$  axis in Fig. 1 is

oriented along the zigzag edge of the graphene sheet. The direction determined by this axis is referred to as the zigzag direction. In turn, the  $oy$  axis is oriented along the armchair-shaped edge and its direction is, correspondingly, referred to as the armchair direction. Both graphene sheets have an almost ideal hexagonal honeycomb structure at this temperature. Almost all Al atoms (except for two atoms) are near the upper graphene sheet at 3300 K (Fig. 1). The Al fragment acquired an irregular loose structure. Some Al atoms are strongly shifted in the vertical direction; i.e., the fragment shape deviates from planar. The structure of the graphene sheets also changes significantly. The upper sheet was deformed to a greater extent (in this sheet, some atoms are not only detached from the main area but also slightly shifted upward to the Al atoms). The corners of the upper sheet are extended; the atoms at the sheet edges lost their linear arrangement in both the armchair and zigzag directions. Some atomic rows in the still-retained regular structure are distorted. The structural changes in the lower graphene sheet are less pronounced. The atom of one of the vertices is detached from the sheet, and there is an indication of a crack along the zigzag direction. The armchair edge was most intensely molten. The atomic rows in the regular-sheet region are slightly distorted.

The relative change in the aluminum-film sizes is shown in Fig. 2. The film begins to be contracted in both the zigzag (curve 1) and armchair (curve 2) directions even at the initial temperature (i.e., at  $T = 300$  K in the calculation). This contraction becomes more intense when reaching a temperature of 800 K. The decrease in the distance between Al atoms at these temperatures is due to the discrepancy between their initial loose packing and the metal density corresponding to the condensed state. In our model, a solid aluminum film containing defects is formed on the graphene surface at low temperatures. The influence of defects can be estimated in the simplest way from the temperature change in the specific heat, because the latter is easier to measure (in comparison with other properties) when the temperature changes rapidly [19]. The isochoric specific heat of the Al film did not increase upon heating; i.e., the influence of defects on the caloric properties was not manifested. The sizes of the metal film in both directions are stabilized in the temperature range  $800 \leq T \leq 2300$  K. A further heating leads to a stable increase in the film size in the zigzag direction and an oscillating change in the film size in the armchair direction.

The temperature changes in the radial distribution function in the Al film, constructed for the atom located most closely to the center of the graphene sheet, are illustrated in Fig. 3. The presence of a symmetry center is a necessary condition for correct construction of this function. It can be seen that at  $T = 300$  K the function  $g_{\text{Al-Al}}(r)$  has a number of peaks at  $r \leq 1$  nm

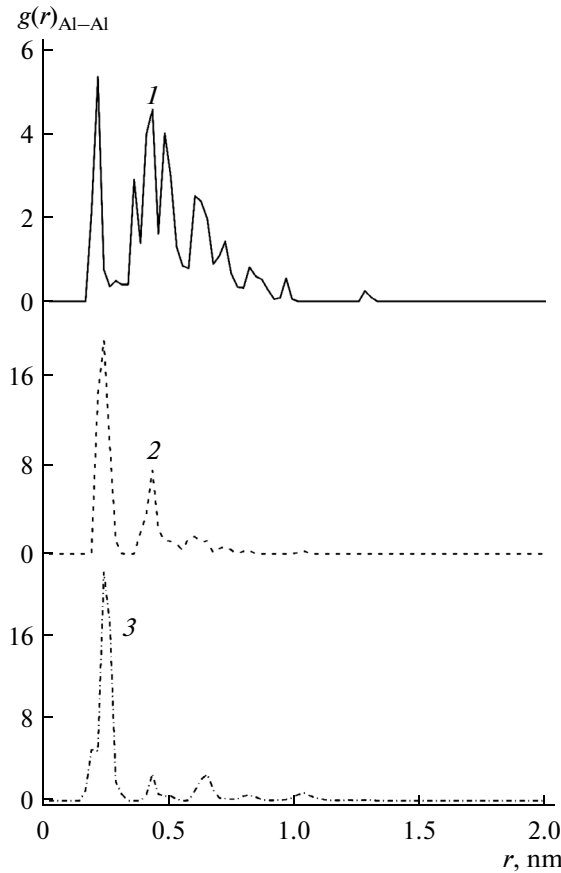


Fig. 3. Radial distribution functions of aluminum film, corresponding to temperatures of (1) 300, (2) 1300, and (3) 3300 K.

(Fig. 3, curve 1). The peak intensity generally decreases with an increase in  $r$ . The film structure in the region of stable film sizes is described by the function  $g_{\text{Al-Al}}(r)$  at  $T = 1300$  K (Fig. 3, curve 2). Here, the function  $g_{\text{Al-Al}}(r)$  exhibits two pronounced peaks at 0.24 and 0.43 nm. The first-peak position is close to the distance between the neighboring atoms in the bulk aluminum crystal (0.2489 nm). At 3300 K, function  $g_{\text{Al-Al}}(r)$  retains only one pronounced peak (Fig. 3, curve 3). The peaks at 0.43 and 0.65 nm are weak. Thus, the increase in temperature reduces the number of well-resolved peaks of the function  $g_{\text{Al-Al}}(r)$  and increases the intensity of its first peak.

The behavior of the mobility of Al atoms on graphene becomes atypical with an increase in temperature (Fig. 4). The horizontal and vertical components of the self-diffusion coefficient  $D$  were calculated from the corresponding squared atomic displacements. The horizontal component  $D_{xy}$  of the self-diffusion coefficient decreases up to a temperature of 1800 K. The component  $D_z$  of this coefficient, which describes vertical atomic displacements, also

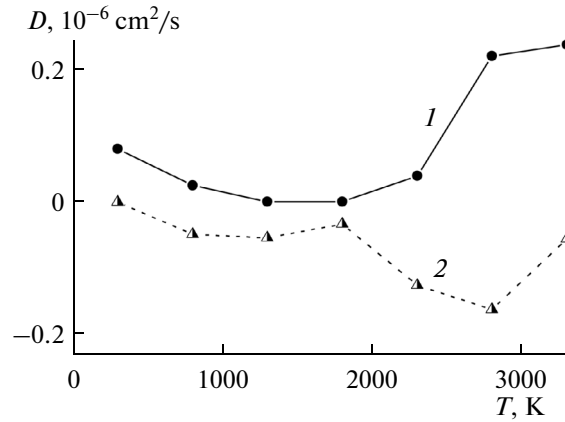


Fig. 4. (1) Horizontal ( $D_{xy}$ ) and (2) vertical ( $D_z$ ) components of the self-diffusion coefficient of Al film.

decreases until the temperature reaches 1300 K. This behavior of the temperature dependence of components  $D_{xy}$  and  $D_z$  is due to the decrease in the distance between Al atoms, which continues up to these temperatures, and the hindrance caused by graphene. At  $T > 1800$  K, component  $D_{xy}$  of the aluminum film increases, whereas the value of component  $D_z$  fluctuates. At these temperatures, the kinetic factor is dominant in comparison with the residual influence of the substrate in the horizontal direction; however, vertical displacements of Al atoms are still hindered due to the attraction by the two-layer graphene. The horizontal component of the self-diffusion coefficient increases significantly when approaching the experimental value of the Al boiling temperature (2773 K), whereas the vertical component of coefficient  $D$  increases only after reaching this temperature.

The nonequivalence of the directions in graphene leads to anisotropy of stresses in the Al-film plane, i.e., the stresses  $\sigma_{xx}$  and  $\sigma_{yy}$  differ significantly (Fig. 5, curves 1, 2). When the forces causing stresses in the film act in the zigzag direction of the graphene sheet, the initial stresses  $\sigma_{xx}$  are the lowest ones and have the shortest relaxation time. The initial stresses in the film increase by a factor of almost 2 in the case where the forces inducing the stress  $\sigma_{yy}$  are oriented parallel to the armchair direction of the graphene sheet. These stresses relax slowly. The highest stresses  $\sigma_{zz}$  in the Al film are induced by the forces acting in the vertical direction. The stresses caused by the vertical forces decrease with an increase in temperature as slowly as stresses  $\sigma_{yy}$ .

The temperature changes in the graphene structure are illustrated in Fig. 6, where one can see the radial distribution functions of C atoms for the upper graphene sheet at three temperatures. As in the case of

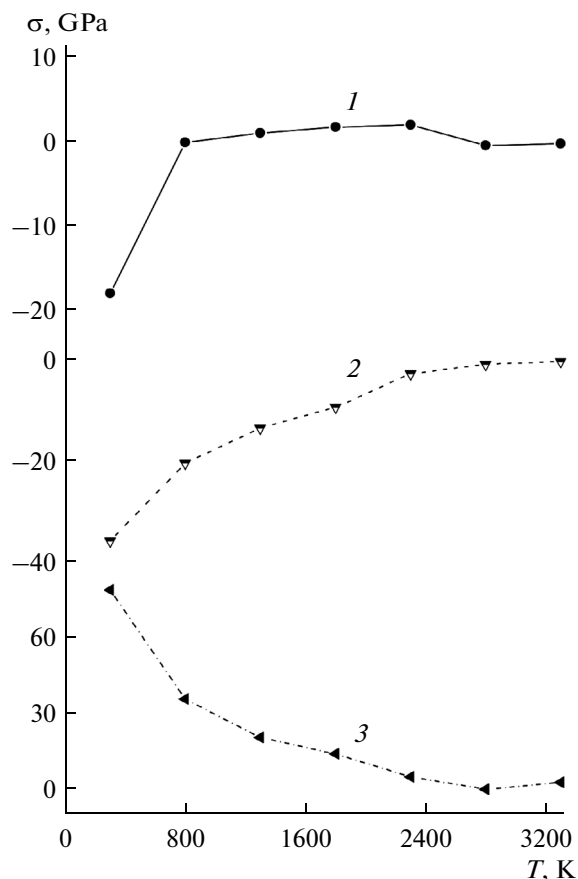


Fig. 5. Stresses in the  $xoy$  plane of Al film: (1)  $\sigma_{zx}$ , (2)  $\sigma_{zy}$ , and (3)  $\sigma_{zz}$ .

Al film, the functions  $g_{C-C}(r)$  were constructed for the single atom located most closely to the sheet center. Many well-resolved peaks of this function at 300 K indicate the presence of an ideal two-dimensional crystal structure. This structure becomes more distorted with an increase in temperature. First of all, this is indicated by the disappearance of the furthest peaks of the function  $g_{C-C}(r)$ . For example, almost all remote peaks, beginning with the sixth one, disappear at  $T = 1300$  K. Only three peaks remain at the temperature of 3300 K. These peaks are shifted to smaller distances with respect to their position at lower temperatures, which is indicative of the presence of denser local atomic packings in the graphene sheet. The long-range order in heated graphene gradually disappears.

The mobility of C atoms in the plane of the lower graphene sheet fluctuates at  $T = 2300$  K (Fig. 7a, curve 2). This behavior of the dependence  $D_{xy}(T)$  can be due to detachment of single C atoms from the sheet corners. However, even at  $T = 2800$  K, the  $D_{xy}$  value for this sheet becomes low again. The  $D_{xy}$  value increases simultaneously for both graphene sheets only at 3300 K; this situation is related to the beginning of fracture of the

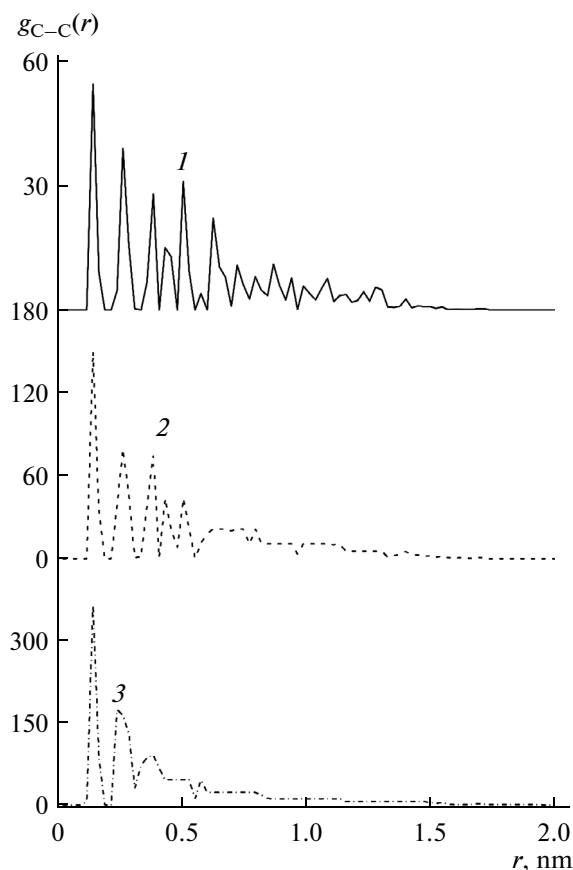
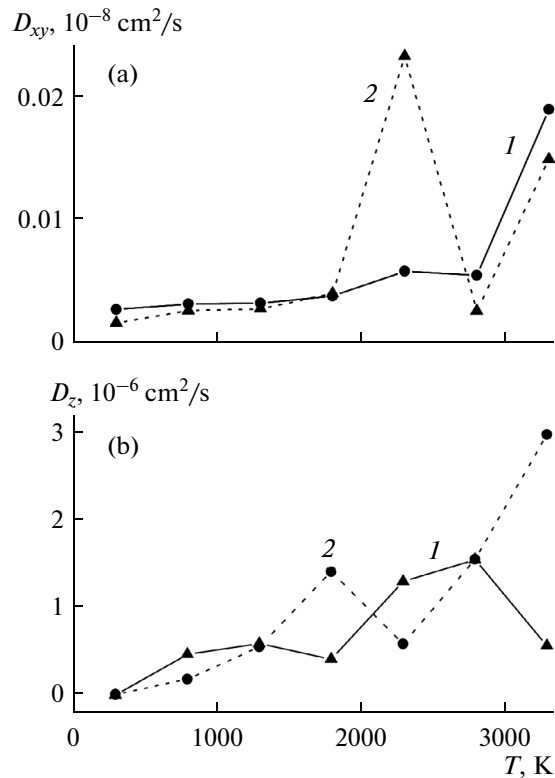


Fig. 6. Radial distribution functions of the upper graphene sheet at temperatures of (1) 300, (2) 1300, and (3) 3300 K.

edges of both sheets. The function  $D_z(T)$  increases with temperature for both sheets more gradually, although this increase is fluctuating. At  $T = 3300$  K, the vertical mobility coefficient of C atoms in the lower sheet increases more rapidly. Although the fluctuations of components  $D_{xy}$  and  $D_z$  for the upper sheet are weaker than those for the lower one, the former, on the whole, appears to be more distorted than the latter.

We will consider how the stresses  $\sigma_{zx}$  and  $\sigma_{zy}$ , formed by atomic rows in the zigzag direction are distributed in the upper graphene sheet (Fig. 8). Even at 300 K (curve 1), the stresses in the sheet plane caused by the forces in the zigzag direction are distributed more nonuniformly than the stresses caused by the forces in the armchair direction. In addition, the stress  $\sigma_{zx}$  has larger maximum amplitudes as compared with the stress  $\sigma_{zy}$ . Since we use free boundary conditions, the amplitude of change in stresses  $\sigma_{zx}$  and  $\sigma_{zy}$  (when passing from one atomic row to another) decreases with an increase in temperature. However, the decrease in the amplitude of this change is more significant for the stresses  $\sigma_{zx}$  (i.e., when the forces act along atomic rows in the zigzag direction).



**Fig. 7.** (a) Horizontal ( $D_{xy}$ ) and (b) vertical ( $D_z$ ) components of the self-diffusion coefficient of the (1) upper and (2) lower graphene sheets.

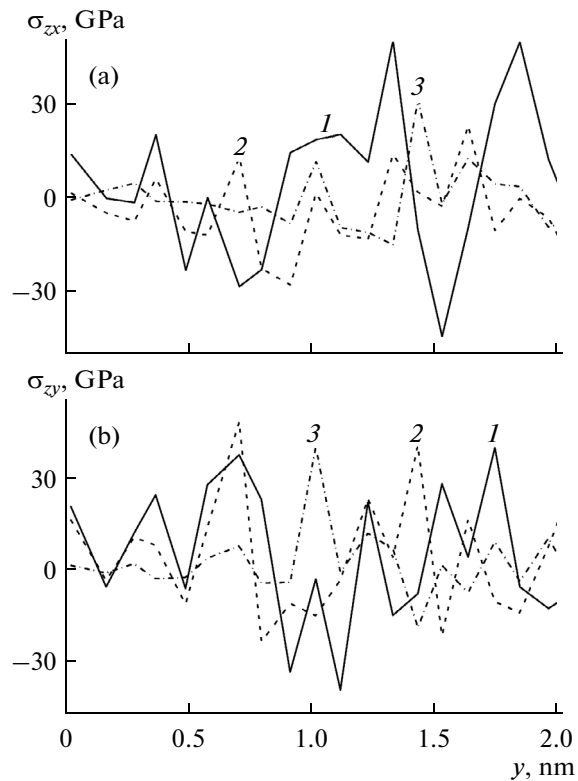


**Fig. 8.** Distribution of stresses (a)  $\sigma_{zx}$  and (b)  $\sigma_{zy}$  in the upper graphene sheet over the rows of C atoms oriented in the zigzag direction at (1) 300, (2) 1300, and (3) 3300 K.

## CONCLUSIONS

Our simulation showed that a monoatomic aluminum film on two-layer graphene has a high thermal stability, which is provided by the high temperature stability of the graphene structure and high absorption properties of graphene. Al atoms freely move over the substrate surface to form a close-packed monolayer island. The size of the metal film decreases more significantly in the transverse direction (the armchair direction with respect to graphene). Below some temperature, a decrease in the distance between the metal atoms that are bonded with the substrate reduces both the horizontal and vertical components of the self-diffusion coefficient of Al atoms. However, when the film temperature is near the experimental value of the Al boiling temperature, both components of the self-diffusion coefficient increase. The stress caused by the longitudinal forces (in the zigzag direction) relaxes in the Al film with the highest rate. The stresses induced by the forces acting in the vertical and armchair directions undergo slow temperature relaxation. The long-range order in two-layer graphene is gradually violated upon heating. However, the graphene sheets under study can be considered as a system with a mid-range order even at 3300 K. There is no explicit correlation between the kinetic properties of aluminum film and graphene sheets. The horizontal mobility of C atoms sharply increases at  $T = 3300$  K (which is in agreement with the behavior of the function  $D_{xy}(T)$  for aluminum), whereas the vertical mobility of C atoms is rather ambiguous. The stress in the plane of the upper graphene sheet caused by the forces acting in the zigzag direction changes (decreases) with an increase in temperature more significantly than the corresponding stress caused by the forces acting in the armchair direction.

## REFERENCES

1. Liu, Q., Liu, Z., Zhang, X., Zhang, N., Yang, L., Yin, S., and Chen, Y., *Appl. Phys. Lett.*, 2008, vol. 92, p. 223303.
2. Hong, W.J., Xu, Y.X., Lu, G.W., Li, C., and Shi, G.Q., *Electrochem. Commun.*, 2008, vol. 10, p. 1555.
3. Liu, Z.F., Liu, Q., Huang, Y., Ma, Y.F., Yin, S.G., Zhang, X.Y., Sun, W., and Chen, Y.S., *Adv. Mater.*, 2008, vol. 20, p. 3924.
4. Hartley, O.N., Russell, R., Heasman, K.C., Mason, N.B., and Bruton, T.M., in *The 29th International Electrical and Electronic Engineering (IEEE) Photovoltaic Specialists Conference (PVSC), New Orleans, Louisiana, United States, May 20–24, 2002*, New Orleans, 2002, paper 103.2.
5. Novoselov, K.S., McCann, E., Morozov, S.V., Falco, V.I., Katsnelson, M.I., Zeitler, U., Jiang, D., Schedin, F., and Geim, A.K., *Nat. Phys.*, 2006, vol. 2, p. 177.

6. Stankus, S.V., Savchenko, I.V., Agadzhanov, A.Sh., Yatsuk, O.S., and Zhmurikov, E.I., *High Temp.*, 2013, vol. 51, no. 2, p. 177.
7. Basharin, A.Yu., Lysenko, I.Yu., and Turchaninov, M.A., *High Temp.*, 2012, vol. 50, no. 4, p. 464.
8. Meyer, J.C., Geim, A.K., Katsnelson, M.I., Novoselov, K.S., Obergfell, D., Roth, S., Girit, C., and Zettl, A., *Solid State Commun.*, 2007, vol. 143, p. 101.
9. Gibertini, M., Tomadin, A., Polini, M., Fasolino, A., and Katsnelson, M.I., *Phys. Rev. B*, 2010, vol. 81, p. 125437.
10. Tersoff, J., *Phys. Rev. B*, 1989, vol. 39, p. 5566.
11. Stuart, S.J., Tutein, A.V., and Harrison, J.A., *J. Chem. Phys.*, 2000, vol. 112, p. 6472.
12. Rafii-Tabar, H., *Phys. Rep.*, 2000, vol. 325, p. 239.
13. Fang, T.-H. and Wu, J.-H., *Comp. Mater. Sci*, 2008, vol. 43, p. 785.
14. Lee, W., Jang, S., Kim, M.J., and Myoung, J.-M., *Nanotechnology*, 2008, vol. 19, p. 85701.
15. Yu, E.K., Stewart, D.A., and Tiwari, S., *Phys. Rev. B*, 2008, vol. 77, p. 195406.
16. Wander, M.C.F. and Shuford, K.L., *J. Phys. Chem.*, 2010, vol. 114, p. 20539.
17. Berendsen, H.J.C., Postma, J.P.M., van Gunsteren, W.F., DiNola, A., and Haak, J.R., *J. Chem. Phys.*, 1984, vol. 81, p. 3684.
18. Davydov, S.Yu., *Fiz. Tverd. Tela*, 2012, vol. 54, no. 4, p. 875.
19. Chekhovskoi, V.Ya. and Peletsky, V.E., *High Temp.*, 2011, vol. 49, no. 1, p. 45.

*Translated by A. Sin'kov*